Spintronic detection of interfacial magnetic switching in a paramagnetic thin film of tris(8-hydroxyquinoline)iron(III)

Dali Sun,[1,*] Christopher M. Kareis,[2] Kipp J. van Schooten,[1] Wei Jiang,[3] Gene Siegel,[3] Marzieh Kavand,[1] Royce A. Davidson,[2] William W. Shum,[2] Chuang Zhang,[1] Haoliang Liu,[1] Ashutosh Tiwari,[3] Christoph Boehme,[1] Feng Liu,[3] Peter W. Stephens,[4] Joel S. Miller,[2] and Z. Valy Vardeny[1,†]

[1]*Department of Physics & Astronomy, University of Utah, Salt Lake City, Utah 84112, USA*
[2]*Department of Chemistry, University of Utah, Salt Lake City, Utah 84112, USA*
[3]*Department of Material Science & Engineering, University of Utah, Salt Lake City, Utah 84112, USA*
[4]*Department of Physics & Astronomy, Stony Brook University, Stony Brook, New York 11794, USA*

(Received 26 May 2016; revised manuscript received 11 November 2016; published 17 February 2017)

Organic semiconductors find increasing importance in spin transport devices due to the modulation and control of their properties through chemical synthetic versatility. The organic materials have been used as interlayers between two ferromagnet (FM) electrodes in organic spin valves, as well as for magnetic spin manipulation of metal-organic complexes at the molecular level. In the latter, the substrate-induced magnetic switching in a paramagnetic molecule has been evoked extensively but studied by delicate surface spectroscopies. Here we present evidence of the substantial magnetic switching in a thin film of the paramagnetic molecule, tris(8-hydroxyquinoline)iron(III) (Feq_3) deposited on a FM substrate, using the magnetoresistance response of electrical spin-injection in an organic spin valve structure, as well as the inverse-spin-Hall effect induced by state-of-art pulsed microwave spin-pumping. We show that interfacial spin control at the molecular level may lead to a macroscopic organic spin transport device, thus bridging the gap between organic spintronics and molecular spintronics.

DOI: 10.1103/PhysRevB.95.054423

I. INTRODUCTION

Organic semiconductors (OSEC) have attracted intense attention for potential applications in spintronic-based devices because of the long spin relaxation time obtained for spin ½ carriers [1–3]. To date, organic spintronics research has focused on the physics of the spin injection and spin transport through the organic interlayer in organic spin valve (OSV) devices. Detection of spin transport through the OSEC layer has been done through a variety of techniques that include magnetotransport [3–12], inverse spin Hall effect (ISHE) [13,14], muon spin rotation [15,16], and two-photon photoemission [17–19]. In most applications, the spin control in the device has been achieved via the injected spin-aligned carriers from conventional FM electrodes into the OSEC interlayer, in spite of the conductivity mismatch at their interface that poses a formidable barrier for spin injection [20].

In contrast to organic spintronics, molecular spintronics utilizes the chemical versatility of molecules; in particular those that have paramagnetic metal ions for manipulating the spin states [21–29]. One particularly promising class of building blocks for molecular spintronics devices is the metalloporphyrins, which exhibit an intrinsic remnant magnetization when in contact with a FM metallic electrode [24], similar to single molecule magnets [30]. Recently, metallophthalocyanines (e.g., CuPc [28], MnPc [31]) also have been intensely studied due to their potential highly spin polarized surface spins ("spinterface") that can act as a spin filter. However, the spin orientation of the molecular ensemble, which is crucial to the ability of spin filtering, was investigated only in the limit of monolayer using a variety of surface science techniques [24–32].

Here we report a spin current-based detection scheme of a molecular spin ensemble by incorporating the paramagnetic semiconductor tris(8-hydroxyquinoline)iron [33] (Feq_3; shown in Fig. 1(a) and Supplemental Material Figs. S1–S3 [34]) as an interlayer into two macroscopic spintronic devices: (i) a ferromagnet (FM)/Feq_3/Au trilayer configuration (OSV-like device) using magnetoresistance response from electrically injected spin aligned carriers; and (ii) a FM/Feq_3/Pt trilayer configuration for ISHE response using microwave (MW) pumped pure spin current. The Feq_3 layer in the OSV-like device functions as a spin filter, but surprisingly it also exhibits a switching field that mimics the coercive field of a conventional FM film. Consequently, the device magnetoresistance response, MR(B), shows similar features to that of a more conventional OSV device. Using superconducting quantum interference device (SQUID) magnetometry, we verified the substantial magnetic ordering and switching that occur in the Feq_3 layer, which is attributed to an indirect antiferromagnetic (AFM) exchange interaction with the FM metallic electrode in the device. Due to this AFM exchange, the NiFe/Feq_3 layer in an ISHE device generates a pure spin current having an *opposite* direction of spin polarization to the magnetization of the NiFe substrate, which results in an ISHE response of reverse polarity compared to that of a NiFe/Pt bilayer. Our experimental findings are further supported by first-principles DFT-type calculations.

II. EXPERIMENTAL DETAILS

Compared to the more conventional diamagnetic tris(8-hydroxyquinoline)aluminum (Alq_3), which has been widely

*Current address: Department of Physics, North Carolina State University, Raleigh, North Carolina 27695, USA.
†To whom correspondence should be addressed: val@physics.utah.edu

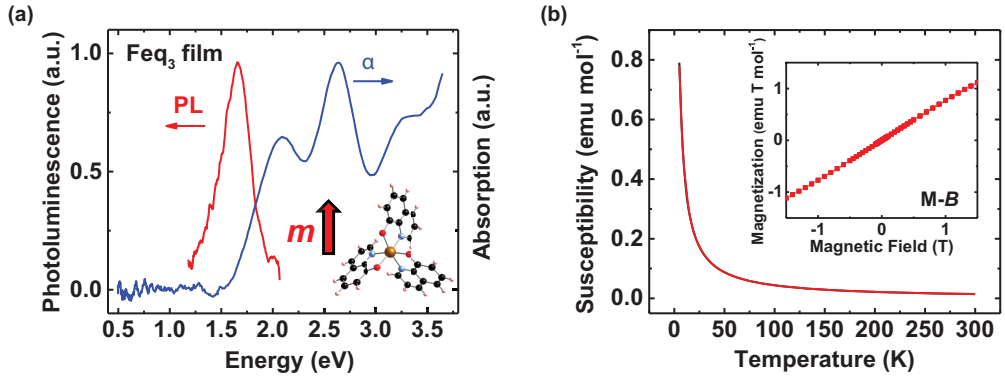

FIG. 1. Feq_3 film properties and basic device characterization. (a) Absorption and photoluminescence spectra of an evaporated Feq_3 thin film on quartz substrate. The inset shows the molecular structure of Feq_3 that contains a Fe^{III} ion having spin, $S = 5/2$ (see also Supplemental Material Fig. S1 [34]). (b) Magnetic susceptibility of a Feq_3 pristine film on quartz as a function of temperature, T, measured by SQUID magnetometer. The inset shows that the resultant M(B) response is characteristic of paramagnetic behaviour.

used as OSEC interlayer in OSV devices [4], Feq_3 has *five electron spins* that originate from the 3*d* transition metal Fe^{III} ion [33] [Fig. 1(a) inset and Supplemental Material Fig. S1 [34]). Therefore, the ground state spin quantum number is $S = 5/2$ [35]. The Feq_3 film is an air-stable semiconductor with an energy gap in the infrared spectral range that results in photoluminescence emission at ∼1.65 eV (∼750 nm) [Fig. 1(a)]. Also, the film exhibits paramagnetic Curie-Weiss susceptibility behavior ($\chi \propto 1/T$) with no detectable hysteresis [Fig. 1(b)]. A schematic structure of the OSV-like device based on a Feq_3 interlayer is illustrated in Fig. 2(a). The device consists of a bottom FM metallic electrode, Feq_3 interlayer film (that was grown *in situ* by thermal evaporation) and capped with a nonmagnetic Au top electrode; a magnetic field, $\boldsymbol{B}$, is applied parallel to the device substrate. For the ISHE measurements, the Au cap electrode is replaced by Pt metal film, which, due to its large spin-orbit coupling, is used for detecting spin currents.

We fabricated the OSV-type devices on two types of bottom FM electrodes. One is a half-metal FM $La_{0.67}Sr_{0.33}MnO_3$ (LSMO) thin film that was epitaxially grown on $SrTiO_3$ substrates by pulsed laser deposition and fabricated for a bottom electrode using conventional wet-etch optical lithography. Another is the $Ni_{80}Fe_{20}$ bottom electrode that was grown by e-beam evaporation through a shadow mask on Si_3N_4 (400 nm)/Si substrates in a vacuum chamber devoted for metal deposition. The FM electrodes were subsequently transferred without breaking the vacuum into a second chamber devoted to OSEC deposition. The Alq_3 (Aldrich) and Feq_3 (synthesized by literature method [33]) films were grown *in situ* by thermal evaporation. The fabricated structures were transferred back to the metal deposition chamber for e-beam evaporation of an Au top electrode (25 nm) in a crossbar configuration. Typical device area was ∼200 × 500 μm.

For an ISHE-type device, an Al thin film electrode (150 nm) was first grown on a glass template (3 × 50 mm) by sputtering using conventional optical lithography. Subsequently two Cu contacts (30 nm thick) with a gap of 3 mm (extended from an Al bottom electrode) were grown by e-beam evaporation through a shadow mask, followed by a strip of Pt electrode (3.5 mm × 1 mm × 7 nm). Without breaking the vacuum, the fabricated structures were transferred with another shadow mask to the organic deposition chamber for OSEC deposition. The OSEC deposition was similar to that used for the OSV-like device. Then the ferromagnetic layer ($Ni_{80}Fe_{20}$, 15 nm), SiO_2 (500 nm) dielectric layer, and top Cu thin film (30 nm) were all grown in series on the OSEC layer by e-beam evaporation through a shadow mask on the OSEC materials.

Transport measurements were performed using a Quantum Design Physical Property Measurement System (PPMS-9) combined with a Keithley 2400 source meter. The magnetic field, B, was applied parallel to the device substrate. The MR is defined as $MR(B) = [R(B) - R(0)]/R(0)$, where $R(0)$ is the junction resistance at $B = 0$, and $R(B)$ is the resistance measured at field B using the four-points method. The magnetization measurements for the susceptibility and devices were performed using the Quantum Design MPMS-5 5 T SQUID magnetometer. The *p*-ISHE measurements were carried out at room temperature in a Bruker ElexSys E580 X-band (∼9.7 GHz) pulsed EPR spectrometer equipped with a dielectric resonator (Bruker FlexLine ER 4118 X-MD5). The MW pulse duration time was set to 2 μs at a repetition rate of 500 Hz. The maximum pulsed MW power was ∼1 kW, resulting in an excitation field amplitude $B_1 = 1.1$ mT at the sample location. The *p*-ISHE(B) response measurements and time dynamics required averaging over 10 240 shots. First-principles calculations were carried out using local spin density approximation (LSDA) with onsite Coulomb interactions and projector augmented-wave method in Vienna *ab-initio* simulation package (VASP) based on density functional theory (DFT), in which an additional on-site Hubbard-U term is included on the iron (III) ($U = 6.0$ eV, $J = 0.9$ eV). The DFT-D2 method [35] was applied to describe the van der Waals interactions that may influence molecular absorption and geometries.

III. RESULTS AND DISCUSSION

A. Magnetoresistance measurements

Typical MR(B) responses of various OSV-like FM/Feq_3 devices with various FM substrates are presented in Figs. 2(b) and 2(c). The MR(B) response of the NiFe/Feq_3 device has

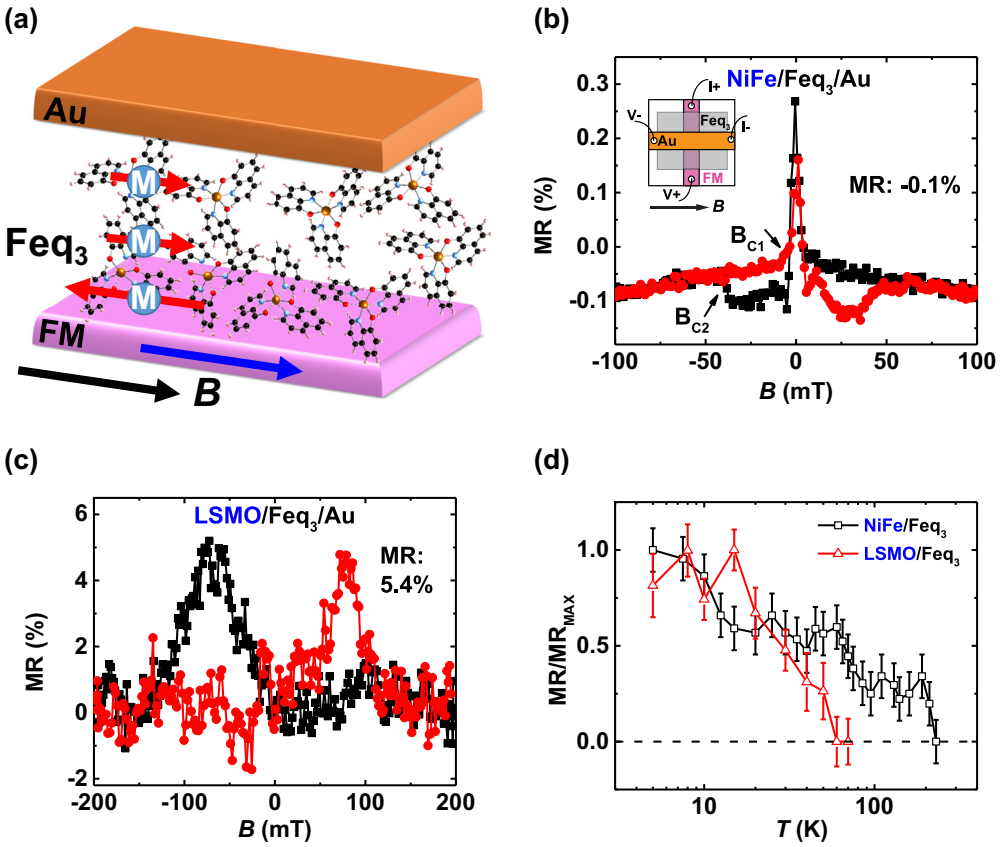

FIG. 2. MR(B) response of various OSV-like devices having a single FM electrode achieved via electrical spin-injection from the FM electrode. (a) Schematic structure of an OSV-like device that consists of a FM bottom electrode, organic spin filter layer (Feq_3), and capped with a nonmagnetic Au electrode. The external magnetic field $\boldsymbol{B}$ is applied parallel to the film. Spin aligned carriers of both spin orientations are injected from the FM electrode and undergo spin filtering by the Feq_3 layer (where one spin orientation is filtered) before reaching the Au electrode. At the interface Feq_3 molecules present an opposite magnetic ordering respect to the bottom FM electrode. The blue arrow indicates the magnetization direction in the FM electrode. (b) and (c) Typical MR(B) responses of NiFe-based and LSMO-based OSV-like devices at 5 K, respectively, with the same Feq_3 spacer thickness (50 nm). B_{C1} and B_{C2} indicate the switching field of the bottom FM electrode and Feq_3 layer, respectively. The inset of (b) illustrates the device geometry for MR measurements. (d) MR_{max} of NiFe and LSMO-based OSV-like devices vs temperature, normalized to MR_{max} at 5 K.

two different response components. The jump of ∼0.2% is observed when the FM substrate magnetization switches at the coercive field, $B_{C1} \approx 3$ mT. This is due to the anisotropic MR(B) response of the NiFe electrode (see Supplemental Material Fig. S4 [34]). The broad negative response of ∼0.1% is due to MR(B) due to spin current through the device. The maximum MR(B) value, MR_{max}, obtained in this OSV-like device, is comparable to NiFe-based conventional OSV devices [15,16]. Surprisingly, we observed that the MR(B) response switches back to the low resistance state at $B = B_{C2} \sim 50$ mT, showing a similar response to that observed in conventional OSV, although only a single FM electrode is used here as opposed to two FM electrodes in more traditional OSV devices. This indicates that an unusual magnetic ordering occurs in the Feq_3 layer when it is placed near a FM substrate, which is modulated by the external field. As a control experiment, upon replacing the bottom NiFe electrode by an Au electrode to form an Au/Feq_3/Au diode, no MR response was obtained (Supplemental Material Fig. S5 [34]). This excludes the possibility that the MR(B) response here is caused by the organic MR (OMAR) [36] or δB mechanism in the Feq_3 layer [37].

When replacing the bottom NiFe electrode by LSMO that is a half-metal FM (see Supplemental Material Fig. S6 for I-V characteristics [34]), which has ∼100% spin aligned carrier injection capability [38], then the obtained MR_{max} [after the nonhysteresis linear MR(B) response that originates from the LSMO electrode [39] was subtracted out; Supplemental Material Fig. S7 [34]] is enhanced by an order of magnitude reaching ∼5.4% [Fig. 2(c)], and the switching field, B_{C2} increases to ∼100 mT. The larger MR_{max} observed for the LSMO-based OSV-like device indicates that the spin aligned carrier injection into the OSEC interlayer has occurred, consistent with the different abilities of NiFe and LSMO FM electrodes to inject spin aligned carriers into an OSEC. The Coulomb blockade induced magnetoresistance cannot explain our observations either since it usually occurs at very low temperature (below 1 K) [40,41]. We note that the MR response in LSMO-based device has opposite polarity compared to that of NiFe-based device. This may be due to the interaction of the Feq_3 molecules and FM electrode at the interface caused by the relative alignment of the Feq_3 HOMO/LUMO and the FM electrode's Fermi level [12].

We also measured the MR(B) response in both NiFe and LSMO-based OSV-like devices at different temperatures, T.

MR_{max} vs T for these devices is summarized in Fig. 2(d). Similar to conventional OSV devices [4], MR_{max} decreases steeply with increasing T and vanishes at 100 K for the LSMO-based OSV-like devices. In contrast, the MR response in the NiFe/Feq_3/Au device survives up to 200 K. We conclude from the various MR(B) and MR_{max} responses vs temperature and voltage (Supplemental Material Fig. S9 [34]) that the OSV-like devices based on Feq_3 interlayer behave very similarly to conventional OSV devices that contain two FM electrodes. Therefore, the OSV-like device may be considered as a simplified version of OSV, which is based on a single FM electrode [42,43].

B. Magnetization measurements

At variance with the previously reported FM ordering in metalloporphyrins and metallophthalocyanines monolayer detected by surface science techniques [24–26], a substantial FM ordering of the Feq_3 layer in the OSV-like device configuration was observed using conventional magnetometry SQUID measurements, i.e., M(B) response (Fig. 3), which may explain the OSV-like MR response of FM/Feq_3/Au trilayers. First, we observed that the M(B) response of a pristine NiFe film [Fig. 3(a)] shows an abrupt hysteretic response at $B < 2$ mT, consistent with its coercive field, B_{C1}. Next we observed the magnetization response of Feq_3 based structures. Compared to the linear paramagnetic response of pristine Feq_3 film having $S = 5/2$ in the ground state [Fig. 1(b)], the M(B) loops of NiFe/Feq_3 and LSMO/Feq_3 OSV-like film structures clearly show a second hysteretic transition (B_{C2}) at a higher field [Figs. 3(b) and 3(d)]. This is distinct from the abrupt transition of the NiFe (or LSMO) electrode seen at low field. As a control experiment, M(B) loops of NiFe/Alq_3 and LSMO/Alq_3 exhibit only the M(B) response feature at B_{C1} that originate from the FM substrate [Figs. 3(c) and 3(e)]. This indicates that the observed MR(B) and M(B) response at B_{C2} cannot be attributed to the π orbitals/substrate hybridization from the hydroxyquinoline ligands [18,19,44]. We note that the narrow hysteresis response of the NiFe electrode at $\sim B_{C1}$ is broader in the OSV-like film structures than that of the pristine NiFe film. This magnetic hardening originates from the OSEC overlayer and is consistent with the enhanced exchange interaction found previously for π-conjugated molecules deposited on FM surfaces due to the proximity of the molecules to the FM atoms [45].

The M(B) responses of NiFe/Feq_3 OSV-like film structures measured upon cooling under two different and opposite magnetic fields of +300 mT and −1 T are shown in Fig. 3(f). The M(B) response asymmetry with respect to $B = 0$ is seen when the field is swept in one direction and then to the opposite direction. This indicates the presence of a magnetic exchange bias [46–49], which results from an AFM coupling [24] at the interface between the Feq_3 and NiFe layers. We note that π-conjugated nonmagnetic organic molecules deposited on FM metallic film show only a symmetric M(B) response [4,12,45]. Reorientated easy axis on the surface of

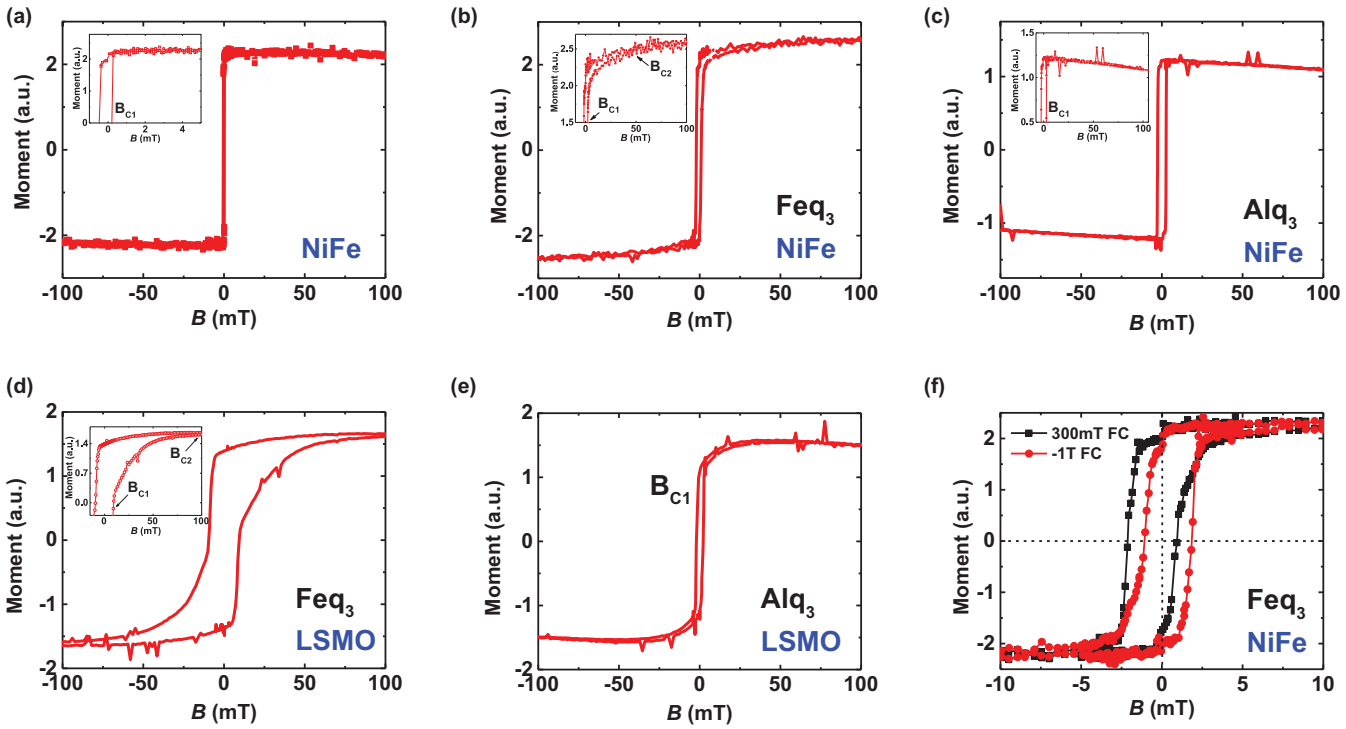

FIG. 3. The SQUID magnetometry of OSV-like device structures. (a)–(e) M(B) response for NiFe, NiFe-Feq_3, NiFe-Alq_3, LSMO-Feq_3, and LSMO-Alq_3 structures, respectively, plotted up to ±100 mT. The insets in (a)–(c) magnify the M(B) response that exhibits additional hysteresis response of the deposited Feq_3 film onto the NiFe substrate. (b) The abrupt transition due to the FM substrate and broad transition from the Feq_3 layer are denoted as B_{C1} and B_{C2}, respectively, which is consistent with the MR(B) response in Fig. 2(b). (f) M(B) responses of NiFe-Feq_3 that are cooled down under two different fields with opposite polarities, plotted up to ±10 mT. All M(B) measurements were performed at 5K.

NiFe/Feq_3 layer from in-plane to out-of-plane can be ruled out because the total magnetization along the in-plane direction is unchanged in opposite field cooling. We conclude that the SQUID magnetometry measurements conclusively reveal that the paramagnetic Feq_3 layer in the proximity of the FM substrate is *magnetically ordered*, consistent with the observed MR(B)-type response of the OSV-like devices. The resulting magnetic switching of the remnant field in the Feq_3 layer occurs at $B_{C2} > B_{C1}$, and this generates the OSV-like MR(B) response in the OSV-like devices.

C. ISHE measurements

Further evidence for an AF order of the Feq_3 layer deposited on a FM substrate is provided by the ISHE. Figure 4(a) demonstrates the working principle and schematic structure of an ISHE device based on Feq_3 molecules. The magnetization dynamics $\boldsymbol{M}(t)$ under ferromagnetic resonance (FMR) condition induces a pure spin current ($\boldsymbol{J}_S$) in the adjacent nonmagnetic Pt layer via spin pumping [50]. Since Pt has a large spin Hall angle ($\theta_{SH} \sim 0.06$) [51], the induced spin current therefore leads to a related electric field, $\boldsymbol{E}_{ISHE}$ perpendicular to both $\boldsymbol{J}_S$ and the spin polarization $\boldsymbol{S}$, namely $\boldsymbol{E}_{ISHE} = \theta_{SH}\boldsymbol{J}_S \times \boldsymbol{S}$. We have used a state-of-the-art pulsed MW excitation [52] to deliver high MW power (~1 kW) to the FM substrate that consequently generates high spin current density in the Pt layer with minimum thermal/resonant heating effect (see Supplemental Material Fig. S11 [34] and Ref. [53]). With the pulsed ISHE (p-ISHE) method, it is possible to investigate a Spinterface feature that occurs in the Feq_3 layer only several molecular monolayers thick.

The inset of Fig. 4(b) shows the p-ISHE voltage generated from a NiFe/Pt ISHE device without Feq_3, measured at room temperature with an in-plane (i.e., $\theta_B = 0°$) field, $\boldsymbol{B}$, as illustrated in Fig. 4(a). The p-ISHE response ($\mathbf{V}_{ISHE} \sim -1.3$ mV at $\theta_B = 0°$) is about two orders of magnitude larger than that of the cw-ISHE due to the high pulsed MW excitation intensity [52]. Possible heating effect can be excluded here since its resulting magnetic field response is independent of the $\boldsymbol{B}$ direction, in sharp contrast with the asymmetric p-ISHE response at $\theta_B = 0°$ and $\theta_B = 180°$ seen in Fig. 4(a) [52,53]. When a 7 nm thick Feq_3 layer (~7 monolayers) is inserted between the NiFe and Pt layers, the observed p-ISHE response from the Pt layer is reduced to ~76 μV [Fig. 4(c)]; see also Supplemental Material Fig. S12 [34]. Importantly, the p-ISHE polarity (at $\theta_B = 0°$ and $\theta_B = 180°$) is *reversed* [Fig. 4(c)] compared to the response without the Feq_3 interlayer. The p-ISHE magnitude and polarity would not change if the spin current would be directly generated from the NiFe layer into the Pt layer via pinholes. We thus conclude that the observed p-ISHE(B) response in the NiFe/Feq_3/Pt structure originates from the spin current that is generated into the Pt layer from the Feq_3 layer itself; we note that spin-pumping from a paramagnetic layer was recently demonstrated [54].

Due to the AFM exchange interaction between the NiFe and Feq_3 layer that is manifested in the MR(B) and SQUID measurements, we conclude that the induced Feq_3 magnetization, $\boldsymbol{m}$, is opposite to $\boldsymbol{M}$. Consequently $\boldsymbol{m}$ in the Feq_3 layer precesses in the opposite direction under the influence of the dynamic magnetization $\boldsymbol{M}(t)$ in the NiFe layer, thereby generating magnons with opposite spin $\mathbf{S}$ respect to those in the NiFe layer. The generated magnons, in turn produce spin current at the Feq_3/Pt interface having opposite spin direction to that produced without the Feq_3 layer; therefore, $\boldsymbol{E}_{ISHE}$ in the Pt layer reverses polarity [see right panel in Fig. 4(a)]. We also note that the electron paramagnetic resonance for the paramagnetic Feq_3 molecules measured at the MW frequency that we use here (~9.7 GHz) is ~300 mT ($g \approx 2$), which differs substantially from the obtained FMR in the NiFe layer (107 mT) and NiFe/Feq_3 bilayer (111 mT). We also measured the p-ISHE responses in a trilayer with smaller Feq_3 thickness (~5 nm) (Supplemental Material Fig. S13 [34]). We confirm that the p-ISHE polarity in this device is still reversed compared to the NiFe/Pt device. In addition, the p-ISHE response is larger (~93 μV) due to the enhanced exchange coupling at smaller Feq_3 thickness. We therefore conclude

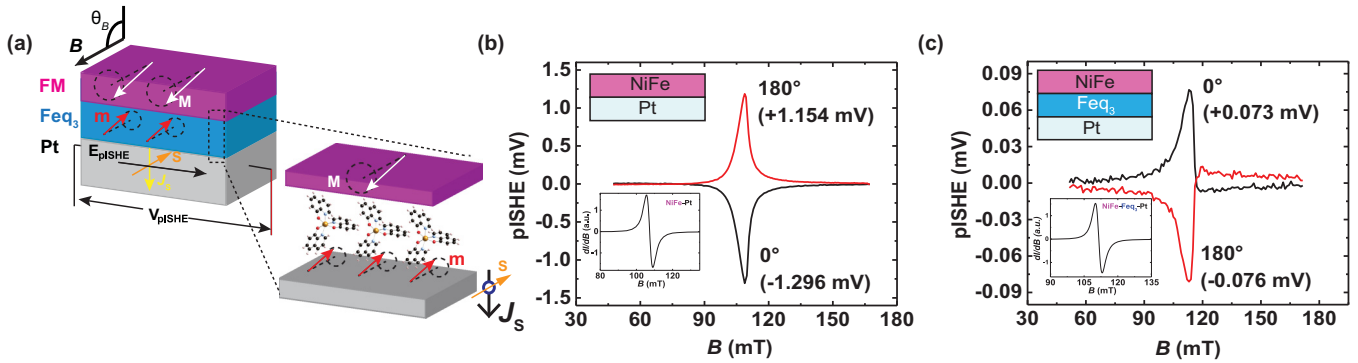

FIG. 4. Pulsed-ISHE(B) response in various Feq_3-based devices generated via spin-pumping. (a) Left panel: schematic illustration (not to scale) of the FM/Feq_3/Pt device. $\boldsymbol{B}$ and $\boldsymbol{M}$ denote, respectively, the static external magnetic field and dynamic magnetization in the FM film that precesses about $\boldsymbol{B}$. $\boldsymbol{J}_S$, $\boldsymbol{S}$, $\mathbf{E}_{ISHE}$, and $\mathbf{V}_{pISHE}$ denote, respectively, the flow of the pulsed spin current, spin polarization vector, generated electric field, and detected p-ISHE voltage. Right panel shows the magnetization precession of the Feq_3 layer, where $\boldsymbol{m}$ and derived $\boldsymbol{S}$ are antiparallel to $\boldsymbol{M}$, under the influence of FM layer via the AFM exchange interaction. (b) and (c) The respective $\mathbf{V}_{pISHE}(B)$ response of NiFe (15 nm)/Pt (10 nm) and NiFe (15 nm)/Feq_3(7 nm)/Pt(10 nm), measured in device structures shown in the insets. All devices are capped with a SiO_2/Cu capacitor layer to suppress the anomalous Hall effect response component [50]. The black and red lines are for in-plane magnetic field $\boldsymbol{B}$(at $\theta_B = 0°$) and $-\boldsymbol{B}$ (at $\theta_B = 180°$), respectively. The lower inset in each panel shows the appropriate FMR(B) response using the same device configuration.

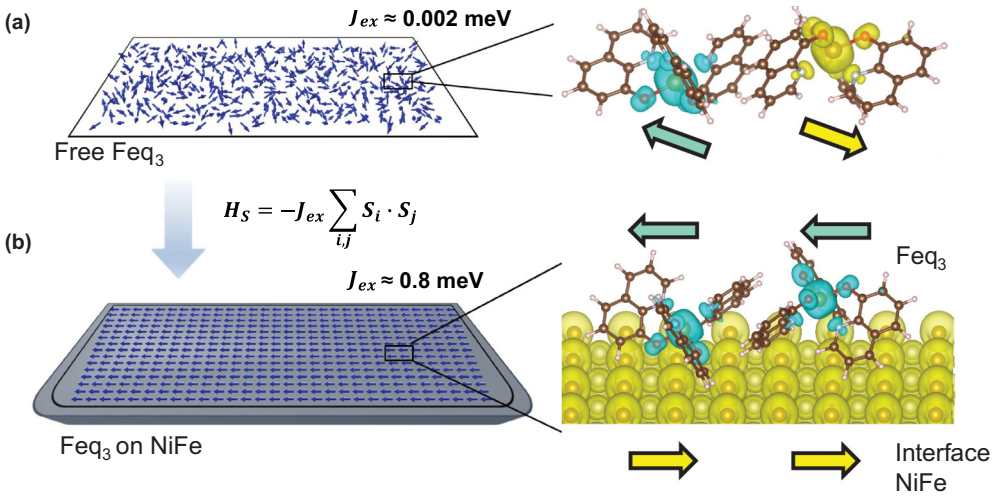

FIG. 5. Theoretical DFT calculations. (a) and (b) The spin density of free Feq_3 molecules and Feq_3 in contact with the NiFe substrate, respectively. The effective coupling constant among the Feq_3 molecules in two systems are labeled, as deduced from Heisenberg spin lattice model. The small dark yellow and light yellow dots represent, respectively, the Fe and Ni atoms of NiFe at the interface. The yellow (blue) spheres denote spins oriented to the right (left side).

that the ISHE measurements provide more direct evidence for a robust AFM exchange interaction between the NiFe and Feq_3 layer, which is consistent with the MR(B) and SQUID measurements in the OSV-like devices.

D. DFT calculation for the interaction between the FM substrate and Feq_3 film

Our conclusion from the measurements above is supported by DFT electronic-structure calculations for the Feq_3 molecules in intimate contact with a FM substrate. To deduce the magnetic ordering strength within the Feq_3 layer in proximity to the FM substrate, we extract the exchange coupling constant (J_{ex}) among the Feq_3 molecules by fitting the Heisenberg spin lattice model to the DFT-calculated energy difference between FM and AFM states (see Supplemental Material section 11 [34]). For a free-standing Feq_3 molecular monolayer [Fig. 5(a)], the energy difference, ΔE between AFM and FM spin configuration is very small ($\Delta E = E_{\mathrm{AFM}} - E_{\mathrm{FM}} < 0.1$ meV, the energy convergence criteria is set at 0.1 meV), which translates to a negligible J_{ex} ($\sim$0.002 meV); this indicates a paramagnetic free-standing Feq_3 layer (Supplemental Material Fig. S15 [34]). However, when the Feq_3 layer is deposited onto the FM NiFe substrate that forms interface layer [Fig. 5(b)], ΔE between AFM and FM spin configuration becomes much larger ($\Delta E = E_{\mathrm{AFM}} - E_{\mathrm{FM}} \sim 8$ meV), and the effective coupling among the Feq_3 molecules changes to strong FM coupling with $J_{ex} \sim 0.8$ meV. This indicates that the paramagnetic Feq_3 layer transitions to weak FM ordering (Supplemental Material Fig. S16a [34]), similar to the Fe-porphyrin layer [24,26]. The origin of FM ordering in the interface Feq_3 can be understood from analysis of the spin-resolved, partial density of state (p-DOS) of the NiFe/Feq_3 system (Supplemental Material Fig. S16b [34]). When the Feq_3 molecules are in close proximity with the NiFe substrate, although there is no direct overlap of Fe^{III} and NiFe d-orbitals, Fe-O, Ni-O and Fe-N, Ni-N interactions exist, as deduced from the spin DOS (Supplemental Material Fig. S16b [34]), which are able to mediate a super-exchangelike interaction. Furthermore, the results of first-principles calculations indicate that interface Feq_3 layer prefers an AFM interface-mediated coupling with the underlying FM NiFe substrate, with an energy difference, $\Delta E = (E_{\mathrm{FM}} - E_{\mathrm{AFM}}) > 25$ meV (Supplemental Material Fig. S16a [34]). This is in agreement with the observed exchange bias in the obtained M(B) response and reversed p-ISHE response (Figs. 3 and 4).

IV. SUMMARY

The discovery of versatile spin filter functionality of Feq_3 thin films and its ability to form an OSV-like device is an important advance for organic spintronics applications. We employed two spin-current based detection themes for studying the magnetic order of Feq_3 layer grown on a FM substrate, namely magnetoresistance and ISHE. We showed that both the OSV-like MR(B) and reversed ISHE(B) response originate from the AFM ordering that occurs at the Feq_3/FM interface. Using a variety of chemical synthesis techniques, incorporation of different transition metals (e.g., Mnq_3, Crq_3, etc.) and other ligands or a proper FM substrate should would enable tuning of the FM/OSEC exchange coupling, as well as the degree of magnetic ordering at the molecular level for altering the magnitude of MR(B), ISHE, and magnetization responses at the macroscopic level.

ACKNOWLEDGMENTS

This paper was supported by the National Science Foundation-Material Science & Engineering Center (NSF-MRSEC; DMR-1121252). The ISHE measurements were supported by the National Science Foundation (DMR-1404634). Use of the National Synchrotron Light Source, Brookhaven National Laboratory was supported by the Basic Energy Sciences, Department of Energy (DE-AC02-98CH10886).

[1] V. A. Dediu, L. E. Hueso, I. Bergenti, and C. Taliani, Spin routes in organic semiconductors, Nat. Mater. **8**, 707 (2009).

[2] D. Sun, E. Ehrenfreund, and Z. V. Vardeny, The first decade of organic spintronics research, Chem. Comm. **50**, 1781 (2013).

[3] S. Pramanik, C.-G. Stefanita, S. Patibandla, S. Bandyopadhyay, K. Garre, N. Harth, and M. Cahay, Observation of extremely long spin relaxation times in an organic nanowire spin valve, Nat. Nanotech. **2**, 216 (2007).

[4] Z. H. Xiong, D. Wu, Z. V. Vardeny, and J. Shi, Giant magnetoresistance in organic spin-valves, Nature **427**, 821 (2004).

[5] J.-W. Yoo, C.-Y. Chen, H. W. Jang, C. W. Bark, V. N. Prigodin, C. B. Eom, and A. J. Epstein, Spin injection/detection using an organic-based magnetic semiconductor, Nat. Mater. **9**, 638 (2010).

[6] T. D. Nguyen, G. Hukic-Markosian, F. Wang, L. Wojcik, X.-G. Li, E. Ehrenfreund, and Z. Valy Vardeny, Isotope effect in spin response of π-conjugated polymer films and devices, Nat. Mater. **9**, 345 (2010).

[7] D. Sun, L. Yin, C. Sun, H. Guo, Z. Gai, X. G. Zhang, T. Z. Ward, Z. Cheng, and J. Shen, Giant Magnetoresistance in Organic Spin Valves. Phys. Rev. Lett. **104**, 236602 (2010).

[8] T. S. Santos, J. S. Lee, P. Migdal, I. C. Lekshmi, B. Satpati, and J. S. Moodera, Room-Temperature Tunnel Magnetoresistance and Spin-Polarized Tunneling through an Organic Semiconductor Barrier, Phys. Rev. Lett. **98**, 016601 (2007).

[9] C. Barraud, P. Seneor, R. Mattana, S. Fusil, K. Bouzehouane, C. Deranlot, P. Graziosi, L. Hueso, I. Bergenti, V. Dediu, F. Petroff, and A. Fert, Unraveling the role of the interface for spin injection into organic semiconductors, Nat. Phys. **6**, 615 (2010).

[10] S. Sanvito, Molecular spintronics: The rise of spinterface science, Nat. Phys. **6**, 562 (2010).

[11] M. Galbiati, Spinterface: Crafting spintronics at the molecular scale, MRS Bulletin, **39**, 602 (2014).

[12] D. Sun, M. Fang, X. Xu, L. Jiang, H. Guo, Y. Wang, W. Yang, L. Yin, P. C. Snijders, T. Z. Ward, Z. Gai, X.-G. Zhang, H. N. Lee, and J. Shen, Active control of magnetoresistance of organic spin valves using ferroelectricity, Nat. Commun. **5**, 4396 (2014).

[13] K. Ando, S. Watanabe, S. Mooser, E. Saitoh, and H. Sirringhaus, Solution-processed organic spin-charge converter, Nat. Mater. **12**, 622 (2013).

[14] S. Watanabe, K. Ando, K. Kang, S. Mooser, Y. Vaynzof, H. Kurebayashi, E. Saitoh and H. Sirringhaus, Polaron spin current transport in organic semiconductors, Nat. Phys. **10**, 308 (2014).

[15] A. J. Drew, J. Hoppler, L. Schulz, F. L. Pratt, P. Desai, P. Shakya, T. Kreouzis, W. P. Gillin, A. Suter, N. A. Morley, V. K. Malik, A. Dubroka, K. W. Kim, H. Bouyanfif, F. Bourqui, C. Bernhard, R. Scheuermann, G. J. Nieuwenhuys, T. Prokscha and E. Morenzoni, Direct measurement of the electronic spin diffusion length in a fully functional organic spin valve by low-energy muon spin rotation, Nat. Mater. **8**, 109 (2009).

[16] L. Schulz, L. Nuccio, M. Willis, P. Desai, P. Shakya, T. Kreouzis, V. K. Malik, C. Bernhard, F. L. Pratt, N. A. Morley, A. Suter, G. J. Nieuwenhuys, T. Prokscha, E. Morenzoni, W. P. Gillin and A. J. Drew, Engineering spin propagation across a hybrid organic/inorganic interface using a polar layer, Nat. Mater. **10**, 39 (2011).

[17] M. Cinchetti, K. Heimer, J.-P. Wüstenberg, O. Andreyev, M. Bauer, S. Lach, C. Ziegler, Y. Gao, and M. Aeschlimann, Determination of spin injection and transport in a ferromagnet/organic semiconductor heterojunction by two-photon photoemission, Nat. Mater. **8**, 115 (2009).

[18] S. Steil, N. Großmann, M. Laux, A. Ruffing, D. Steil, M. Wiesenmayer, S. Mathias, O. L. A. Monti, M. Cinchetti, and M. Aeschlimann, Spin-dependent trapping of electrons at spinterfaces, Nat. Phys. **9**, 242 (2013).

[19] A. Droghetti, S. Steil, N. Großmann, N. Haag, H. Zhang, M. Willis, W. P. Gillin, A. J. Drew, M. Aeschlimann, S. Sanvito, and M. Cinchetti, Electronic and magnetic properties of the interface between metal-quinoline molecules and cobalt, Phys. Rev. B **89**, 094412 (2014).

[20] G. Schmidt, D. Ferrand, L. W. Molenkamp, A. T. Filip, and B. J. van Wees, Fundamental obstacle for electrical spin injection from a ferromagnetic metal into a diffusive semiconductor, Phys. Rev. B **62**, R4790 (2000).

[21] A. R. Rocha, V. M. García-suárez, S. W. Bailey, C. J. Lambert, J. Ferrer, and S. Sanvito, Towards molecular spintronics, Nat. Mater. **4**, 335 (2005).

[22] S. Sanvito, Molecular spintronics, Chem. Soc. Rev. **40**, 3336 (2011).

[23] S. Sanvito, Organic spintronics: Filtering spins with molecules, Nat. Mater. **10**, 484 (2011).

[24] H. Wende, M. Bernien, J. Luo, C. Sorg, N. Ponpandian, J. Kurde, J. Miguel, M. Piantek, X. Xu, Ph. Eckhold, W. Kuch, K. Baberschke, P. M. Panchmatia, B. Sanyal, P. M. Oppeneer, and O. Eriksson, Substrate-induced magnetic ordering and switching of iron porphyrin molecules, Nat. Mater. **6**, 516 (2007).

[25] P. Gambardella, S. Stepano, A. Dmitriev, J. Honolka, F. M. F. de Groot, M. Lingenfelder, S. S. Gupta, D. D. Sarma, P. Bencok, S. Stanescu, S. Clair, S. Pons, N. Lin, A. P. Seitsonen, H. Brune, J. V. Barth, and K. Kern, Supramolecular control of the magnetic anisotropy in two-dimensional high-spin Fe arrays at a metal interface, Nat. Mater. **8**, 189 (2009).

[26] M. Mannini, F. Pineider, P. Sainctavit, C. Danieli, E. Otero, C. Sciancalepore, A. M. Talarico, M.-A. Arrio, A. Cornia, D. Gatteschi, and R. Sessoli, Magnetic memory of a single-molecule quantum magnet wired to a gold surface, Nat. Mater. **8**, 194 (2009).

[27] A. Lodi Rizzini, C. Krull, T. Balashov, J. J. Kavich, A. Mugarza, P. S. Miedema, P. K. Thakur, V. Sessi, S. Klyatskaya, M. Ruben, S. Stepanow, and P. Gambardella, Coupling Single Molecule Magnets to Ferromagnetic Substrates, Phys. Rev. Lett. **107**, 177205 (2011).

[28] M. Warner, S. Din, I. S. Tupitsyn, G. W. Morley, A. M. Stoneham, J. A. Gardener, Z. Wu, A. J. Fisher, S. Heutz, C. W. M. Kay, and G. Aeppli, Potential for spin-based information processing in a thin-film molecular semiconductor, Nature **503**, 504 (2013).

[29] T. Miyamachi, M. Gruber, V. Davesne, M. Bowen, S. Boukari, L. Joly, F. Scheurer, G. Rogez, T. K.Yamada, P. Ohresser, E. Beaurepaire, and W. Wulfhekel, Robust spin crossover and memristance across a single molecule, Nat. Commun. **3**, 938 (2012).

[30] L. Bogani and W. Wernsdorfer, Molecular spintronics using single-molecule magnets, Nat. Mater. **7**, 179 (2008).

[31] F. Djeghloul, F. Ibrahim, M. Cantoni, M. Bowen, L. Joly, S. Boukari, P. Ohresser, F. Bertran, P. Le Fèvre, P. Thakur, F. Scheurer, T. Miyamachi, R. Mattana, P. Seneor, A. Jaafar, C. Rinaldi, S. Javaid, J. Arabski, J.-P. Kappler, W. Wulfhekel *et al.*,

Direct observation of a highly spin-polarized organic spinterface at room temperature, Sci. Rep. **3**, 1272 (2013).

[32] S. Schmaus, A. Bagrets, Y. Nahas, T. K. Yamada, A. Bork, M. Bowen, E. Beaurepaire, F. Evers, and W. Wulfhekel, Giant magnetoresistance through a single molecule, Nat. Nanotech. **6**, 185 (2011).

[33] J. E. Tackett and D. T. Sawyer, Properties and infrared spectra in the potassium bromide region of 8-quinolinol and its metal chelates, Inorg. Chem. **3**, 692 (1964).

[34] See Supplemental Material at http://link.aps.org/supplemental/10.1103/PhysRevB.95.054423 for Feq_3 structure and characterization; anisotropic magnetoresistance response; organic magnetoresistance response; I-V characteristics; non-hysteresis MR(B) background; Feq_3 switching field as a function of temperature and bias voltage; bias dependence of MR response; SQUID measurements in LSMO/Feq_3 OSV-like devices; time (t) and field (B) responses of p-ISHE voltage in the ISHE-type device; broadband FMR spectrum; DFT calculations and model.

[35] W. Jiang, M. Zhou, Z. Liu, D. Sun, Z. V. Vardeny, and F. Liu, Structural, electronic, and magnetic properties of tris(8-hydroxyquinoline)iron(III) molecules and its magnetic coupling with ferromagnetic surface: first-principles study, J. Phys.: Condens. Matter. **28**, 176004 (2016).

[36] Ö. Mermer, G. Veeraraghavan, T. L. Francis, Y. Sheng, D. T. Nguyen, M. Wohlgenannt, A. Köhler, M. K. Al-Suti, and M. S. Khan, Large magnetoresistance in nonmagnetic π-conjugated semiconductor thin film devices, Phys. Rev. B **72**, 205202 (2005).

[37] M. Cox, S. P. Kersten, J. M. Veerhoek, P. Bobbert, and B. Koopmans, ΔB mechanism for fringe-field organic magnetoresistance, Phys. Rev. B **91**, 165205 (2015).

[38] J.-H. Park, E. Vescovo, H.-J. Kim, C. Kwon, R. Ramesh, and T. Venkatesan, Direct evidence for a half-metallic ferromagnet, Nature **392**, 794 (1998).

[39] D. Wu, Z. Xiong, X. Li, Z. V. Vardeny, and J. Shi, Magnetic-Field-Dependent Carrier Injection at $La_{2/3}Sr_{1/3}MnO_3$ and Organic Semiconductors Interfaces, Phys. Rev. Lett. **95**, 016802 (2005).

[40] J. Wunderlich, T. Jungwirth, B. Kaestner, A. C. Irvine, A. B. Shick, N. Stone, K.-Y. Wang, U. Rana, A. D. Giddings, C. T. Foxon, R. P. Campion, D. A. Williams, and B. L. Gallagher, Coulomb Blockade Anisotropic Magnetoresistance Effect in a (Ga,Mn) As Single-Electron Transistor, Phys. Rev. Lett. **97**, 077201 (2006).

[41] M. Urdampilleta, S. Klyatskaya, J. P. Cleuziou, M. Ruben, and W. Wernsdorfer, Supramolecular spin valves, Nat. Mater. **10**, 502 (2011).

[42] K. V. Raman, A. M. Kamerbeek, A. Mukherjee, N. Atodiresei, T. K. Sen, P. Lazić, V. Caciuc, R. Michel, D. Stalke, S. K. Mandal, S. Blügel, M. Münzenberg, and J. S. Moodera, Interface-engineered templates for molecular spin memory devices, Nature **493**, 509 (2013).

[43] K. V. Raman, Interface-assisted molecular spintronics. Interface-assisted molecular spintronics, Appl. Phys. Rev. **1**, 031101 (2014).

[44] Y. Zhan, E. Holmström, R. Lizárraga, O. Eriksson, X. Liu, F. Li, E. Carlegrim, S. Stafström, and M. Fahlman, Efficient spin injection through exchange coupling at organic semiconductor/ferromagnet heterojunctions, Adv. Mater. **22**, 1626 (2010).

[45] M. Callsen, V. Caciuc, N. Kiselev, N. Atodiresei, and S. Blügel, Magnetic Hardening Induced by Nonmagnetic Organic Molecules, Phys. Rev. Lett. **111**, 106805 (2013).

[46] J. Nogués and I. K. Schuller, Exchange bias, J. Magn. Magn. Mater. **192**, 203 (1999).

[47] J. Hong, T. Leo, D. J. Smith, and A. Berkowitz, E. Enhancing Exchange Bias with Diluted Antiferromagnets, Phys. Rev. Lett. **96**, 117204 (2006).

[48] M. Gruber, F. Ibrahim, S. Boukari, H. Isshiki, L. Joly, M. Peter, M. Studniarek, V. Da Costa, H. Jabbar, V. Davesne, U. Halisdemir, J. Chen, J. Arabski, E. Otero, F. Choueikani, K. Chen, P. Ohresser, W. Wulfhekel, F. Scheurer, W. Weber *et al.*, Exchange bias and room-temperature magnetic order in molecular layers, Nat. Mater. **14**, 981 (2015).

[49] C. Nistor, C. Krull, A. Mugarza, S. Stepanow, C. Stamm, M. Soares, S. Klyatskaya, M. Ruben, and P. Gambardella, Exchange bias of TbPc2 molecular magnets on antiferromagnetic FeMn and ferromagnetic Fe films, Phys. Rev B **92**, 184402 (2015).

[50] K. Ando, S. Takahashi, J. Ieda, H. Kurebayashi, T. Trypiniotis, C. H. W. Barnes, S. Maekawa, and E. Saitoh, Electrically tunable spin injector free from the impedance mismatch problem, Nat. Mater. **10**, 655 (2011).

[51] J. C. Rojas-Sánchez, N. Reyren, P. Laczkowski, W. Savero, J. P. Attane, C. Deranlot, M. Jamet, J. M. George, L. Vila, and H. Jaffres, Spin Pumping and Inverse Spin Hall Effect in Platinum: The Essential Role of Spin-Memory Loss at Metallic Interfaces, Phys. Rev. Lett. **112**, 106602 (2014).

[52] D. Sun, K. J. van Schooten, M. Kavand, H. Malissa, C. Zhang, M. Groesbeck, C. Boehme, and Z. V. Vardeny, Inverse spin Hall effect from pulsed spin current in organic semiconductors with tunable spinorbit coupling, Nat. Mater. **15**, 863 (2016).

[53] K. Ando and E. Saitoh, Observation of the inverse spin Hall effect in silicon, Nat. Commun. **3**, 629 (2012).

[54] Y. Shiomi and E. Saitoh, Paramagnetic Spin Pumping, Phys. Rev. Lett. **113**, 266602 (2014).